Real-time TDDFT Investigation of Optical Absorption in Gold Nanowires

Ravithree D. Senanayake[a], David B. Lingerfelt[b], Gowri U. Kuda-Singappulige,[a] Xiaosong Li[b,*] & Christine M. Aikens[a,*]

[a]Department of Chemistry, Kansas State University, Manhattan, KS 66506, USA

[b]Department of Chemistry, University of Washington, Seattle, WA 98195, USA

* cmaikens@ksu.edu, 1-785-532-0954, fax: 1-785-532-6666; xsli@uw.edu, 1-206-685-1804

Abstract

Using a real-time TDDFT method, a set of linear gold nanowires Au_m (m = 4, 6, 8, 10, 12) is investigated to understand the plasmon-like behavior that results from resonant excitation of a superposition of single-electron transitions. These characteristic excitations of gold nanowires have been previously investigated via linear response TDDFT calculations, and the results from these two approaches are compared. Real-time TDDFT provides dynamical information about the how the electron populations change during excitations in these systems. This study also investigates the relationship between the d-band transitions and the plasmon-like states in gold nanowires. In this work, the longitudinal and transverse absorption peaks are studied after dipolar excitation, and the effects of changing the length of the nanowire are examined. The time evolution of the single particle transitions and the interplay between different transitions involved in the plasmon-like excitations of model gold nanowires are also investigated. The lowest-energy longitudinal excitation occurs around 1-2 eV in the optical absorption spectra; this peak redshifts with increasing nanowire length. A splitting in the longitudinal peak is present due to the involvement of interband transitions. The frequency of the transverse mode, which lies around 6-7 eV in the absorption spectra, tends to stay constant as the nanowire length increases. The time dependent occupation numbers and their Fourier transformed spectra reveal that a dominant single particle transition ($\Sigma_n \rightarrow \Sigma_{n+1}$) can be identified in the longitudinal peaks which is coupled with less probable d-band transitions (d $\rightarrow \Sigma$). In contrast, the transverse modes are constructed from a coupling of two or more single particle transitions with $\Sigma_n \rightarrow \Pi_n$ character.

Introduction

Noble metal nanoparticles composed of silver and gold are of interest due their important applications in sensing,[1-9] catalysis,[10] biomedicine,[11-14] and energy conversion and storage.[15-16] Gold nanorods and nanowires can be used in photothermal cancer therapy applications.[12, 17] Noble metal nanoparticles in the size range of 10 – 100 nm exhibit one or more strong absorption peaks in the visible to near IR region, which is an important characteristic of these nanoparticles called the surface plasmon resonance (SPR).[18-22] The SPR phenomenon in gold and silver nanoparticles has been widely studied experimentally[23-26] and theoretically[27-32] because many of their applications rely on this property. The absorption peaks can be tuned by changing the size,[33] shape,[34-35] and the environment[36] of the nanoparticles.

Among the various shapes of nanoparticles available, nanorods and nanowires have drawn significant attention due the high sensitivity of their optical properties to their aspect ratios.[20, 37-38] The two main plasmon resonances present in alkali metal and noble metal nanowires are the longitudinal and transverse modes.[6, 36, 39-42] The longitudinal mode is obtained by applying an electric field polarized along the main axis (*z* direction) of the nanowire. A change in the nanowire length can result in a change in the energy and the intensity of the longitudinal mode.[43] The transverse mode is obtained by applying the field in a direction polarized perpendicular to the main axis such as the *x* direction. Previous investigations on nanorods/nanowires have shown that the longitudinal peak in the optical absorption spectrum tends to redshift in energy with increasing aspect ratio while the transverse mode does not greatly change in energy with increasing aspect ratio.[36, 39-42, 44]

Time dependent density functional theory (TDDFT) has been used to understand the origin of the optical absorption spectra of many noble metal nanoparticles.[28, 41-54] The absorption spectra of small nanoclusters exhibit one or more intense peaks that are similar to the plasmon resonance of larger nanoparticles.[47, 55] Linear response time dependent density functional theory (LR-TDDFT) calculations demonstrate that dipolar plasmon modes in the noble metal nanoclusters can be recognized through the concept of constructive addition of single electron transitions; this is expected to be applicable for both large nanoparticles that are several hundred nanometers in size and smaller nanoparticles with diameters less than 2 nm.[42, 47, 56-58] A different method for

identifying single particle transitions and plasmons that relies on the different behavior of plasmon and single particle transition energies upon scaling of the electron-electron interactions has also been suggested by Jacob and coworkers.[48]

Noble metal nanowires are one class of nanoparticles that have been studied by the TDDFT method.[43-44, 48-52] The plasmon excitations in small nanowires have often been investigated using the frequency domain LR-TDDFT method.[43] Although extremely useful for calculating absorption spectra and determining the transitions responsible, LR-TDDFT calculations do not reveal the dynamical nature of the interplay between the electronic excited states which is vital to understanding the plasmon modes present in nanoclusters. Moreover, the LR-TDDFT method is restricted to the interaction with weak electric fields. Therefore, the real-time TDDFT (RT-TDDFT) method has recently attracted attention as a prominent method to understand the time evolution of molecular systems in the presence of an external perturbation, because it can provide dynamical information and can be applied to systems interacting with strong fields. Moreover, it can be applied to larger systems than those that are currently tractable using the LR-TDDFT approach. Recently, Weerawardene and Aikens provided an overview of the comparison of LR-TDDFT and RT-TDDFT methods for examining the absorption spectra of noble metal nanoparticles.[59]

RT-TDDFT has been used to study the end and central plasmon modes in linear sodium and silver chains by Gao and coworkers.[50-51] Later, Luo et al.[52] investigated the size dependence of electronic excitations in copper, silver and gold chains up to 26 atoms. Recently, the coherent plasmonic behavior of silver nanowires Ag_m (m = 4, 6, 8, 10, 12) was studied by Li and coworkers[60] using a RT-TDDFT method. In the latter study, the interplay between the time evolution of the superposition of the single particle transitions and the plasmonic excitations was investigated. It was shown that the transverse transitions in silver nanowires are collective in nature and oscillate in phase with respect to each other.

While it is more challenging in RT-TDDFT than in LR-TDDFT to identify the single-particle transitions that are responsible for a given excitation, methods have recently been developed that provide insights into the orbitals involved. Li et al. demonstrated that a projection of the time-dependent density matrix onto the initial orbitals can be used to determine time-dependent occupation numbers and identify occupied-virtual pairs involved in the transition.[61]

Other researchers have examined the dynamics of the off-diagonal elements of the density matrix and have used these to investigate electron dynamics after excitation.[62-64] Examination of how electronic population varies over time is an important advantage of the RT-TDDFT approach.

A LR-TDDFT investigation on silver nanowires showed that the longitudinal peak of the silver nanowires corresponds to the HOMO → LUMO transition, which is a Σ → Σ transition (the delocalized frontier orbitals of nanowires can be referenced by the irreducible representations of the $D_{\infty h}$ point group (Σ, Π, Δ, etc.) due to their approximate cylindrical symmetry), whereas the transverse peak is a superposition of several single particle transitions (Σ → Π) adding constructively.[43] This behavior was also observed in similar RT-TDDFT calculations.[60] Until now, there has been no RT-TDDFT investigation performed on the gold nanowires to understand the dynamical nature of the superposition of single particle transitions involved. However, this is important because the plasmon resonance in noble metal nanoparticles can be affected by transitions from the d band. This effect is profound in gold nanoparticles due to relativistic effects that lead to a smaller splitting between the d and sp bands compared to silver and alkali metal nanoparticles.[41, 49, 65] Moreover, because the density of states is higher in gold nanowires, this affects phenomena such as plasmon decay and the formation of hot carriers (hot electrons and holes). In this work, our aim is to understand how the plasmon-like excitations in gold nanowires differ compared to those of silver nanowires using the RT-TDDFT approach. We also aim to understand to what extent transitions out of the d band play a role in determining the character of plasmon-like states in gold nanowires.

Computational Methodology

The current work uses the RT-TDDFT approach to study the interplay between the time evolution of the superposition of the single particle transitions and the plasmonic excitations in model gold nanowires Au_m (m = 4, 6, 8, 10, 12). A step function electric field[66] is utilized as the perturbation to probe the dipole response of the longitudinal and transverse modes upon changing the nanowire length. The step function electric field can be described as follows:

$$E(t) = E_0 \text{ for } t < 0 \quad (t = \text{time})$$

$$E(t) = 0 \text{ for } t > 0$$

In practice, this is done by preparing the initial electron density for the system with a self-consistent field calculation performed in the presence of a static electric field E_0. Then, the field is turned off and the electronic system is propagated using the RT-TDDFT approach.[60] The nature of the plasmon excitation as a superposition of single particle transitions is analyzed through the time evolution of the molecular orbital occupation numbers. The orbital occupation numbers $n_k(t)$ are determined by projecting the time-dependent density matrix $\boldsymbol{P}(t)$ onto the initial orbitals:

$$n_k(t) = \boldsymbol{C}_k^{\dagger}(0)\boldsymbol{P}(t)\boldsymbol{C}_k\,(0)$$

where $\boldsymbol{C}_k\,(0)$ is the k^{th} eigenvector of the initial Kohn-Sham matrix.[61] Anticorrelated time dynamics of the occupation numbers of initially occupied and unoccupied orbitals can be used to identify which single-particle transitions are responsible for the strongest optical absorption peaks. Moreover, the collective oscillation of single particle orbital occupations that are in-phase and coherent will help to identify the collective nature of the plasmon resonance.[60] We compare the analysis using the Fourier transform of the time evolution of the occupation numbers with that obtained for the off-diagonal elements of the density matrix.

RT-TDDFT calculations were performed on a series of linear gold chains having 4, 6, 8, 10 and 12 atoms. A development version of the GAUSSIAN series of programs[67] was used to carry out the real-time simulations. The RT-TDDFT calculations are described elsewhere.[60] The real-time formalization utilizes an approach similar to a full time dependent Hartree-Fock (TDHF) approach developed by Schlegel and coworkers.[61] That method was previously used to understand the effects of a time dependent electric field on the dipole moments, charge distribution and the frontier orbital population in linear polyenes.[68-69] LR-TDDFT calculations are also performed for direct comparison with the RT-TDDFT calculations.

In this work, the BP86[70-71] exchange-correlation functional and the LanL2DZ[72-74] effective core potential basis set were used in all calculations. A simulation time of 120 fs was performed for the longitudinal modes and 480 fs for the transverse modes with an integration step size of 1.2 as. The longer simulation time for the transverse mode was performed to check convergence; it was found that a good convergence in the optical absorption spectrum of the system can be achieved with a simulation time of 120 fs. An external static field was used with a strength of 0.001 a.u.; this field is low enough that the system stays in the weak perturbation regime, thereby

enabling direct comparison with LR-TDDFT calculations. A 150 a.u. damping factor was used during Fourier transformation of the time-dependent dipole moments to obtain the dipole strength function which is proportional to the optical absorption spectrum. The damping factor is used to account for the experimental broadening. The time-dependent dipole moment $\mu(t)$ is calculated at each time step using the equation,

$$\mu(t) = \mathrm{Tr}[\mathbf{DP}(t)]$$

In the orthonormal basis, the dipole matrix is given by **D** and the density matrix is given by **P**. Then, the dipole strength function $S(\omega)$ is given by,[75]

$$S(\omega) = \frac{4\pi\omega\, Tr[\mathrm{Im}\alpha(\omega)]}{3c}$$

where $\alpha(\omega)$ is the polarizability in the frequency domain, which can be obtained by the Fourier transform of the dipole moment $\mu_i(\omega)$ and step electric field $E_i(\omega)$ relation as shown:

$$\mu_i(\omega) = \alpha_{ii}(\omega)E_i(\omega)$$

where *i* indicates the *x, y, z* Cartesian coordinates.

Coordinates for the gold nanowires were obtained from an optimization at the BP86/TZP level of theory with scalar relativistic effects treated by ZORA[76] using the ADF[77] software. The nanowires are positioned so that their coordinates lie along the *z*-axis (see Supporting Information, SI). These linear atomic chains are not minima on the potential energy surface, but can provide insights into the physics of electronic excitations in larger gold nanorods and nanowires. The geometries of the linear chains were held constant during the RT-TDDFT electron dynamics and LR-TDDFT excited state calculations.

Results and Discussion

Dipole strength functions of the longitudinal and transverse modes

The dipole strength functions (optical absorption spectra) that result from applying a step function electric field to five gold nanowires are shown in Fig. 1. The electric field perturbation is applied along the longitudinal (z) and transverse (x) directions. Due to the symmetry of the system,

results for an electric field in the *y* direction (not shown) are the same as the *x* direction. The main peaks in the energy range of 0-8 eV are analyzed for both longitudinal and transverse modes. Unlike in a similar series of silver nanowires[60] where the longitudinal mode appears as a single sharp peak in the energy range of 1-2 eV, several peaks in the optical absorption plots for the gold nanowires indicate that several longitudinal excitations are present. Despite some differences due to the level of theory used, most of the findings related to the optical absorption spectra in this RT-TDDFT study are consistent with the previous LR-TDDFT study on gold nanowires performed by Guidez and Aikens.[43] For example, the LR-TDDFT spectra of gold nanowires display a redshift and several longitudinal excitations at ~2 eV[43] comparable to the peaks observed in the energy range of 2-6 eV in Fig. 1a - e. The Au_4 nanowire exhibits a small peak around 2 eV that redshifts with the increasing number of atoms in the nanowire up to Au_{12}. The peak intensity grows and the peak displays a splitting with increasing length. In the energy range of 3-7 eV, a few low intensity peaks and a high intensity peak are present for Au_4 that also redshift for longer nanowires. The intensities of the peaks around 3 eV significantly increase with length, while the peaks in the 4-7 eV range increase less dramatically in intensity for longer systems. The splitting of the peaks in longer nanowires are due to the transitions originating from the d band, in agreement with the previous LR-TDDFT study on gold nanowires.[43] Redshifting of the longitudinal peak has also been observed for silver nanowires, although in the case of silver only a single strong longitudinal peak is present.[60] Similar to the silver nanowire case,[60] the energy of the transverse peak (6-7 eV) is essentially constant although a small blueshift is apparent as the nanowire length increases. Unlike in silver, the gold nanowires exhibit several transverse peaks as well as several longitudinal excitations. For both excitation modes, the dipole strength increases as the nanowire length grows. This has also been observed for other elongated systems such as pentagonal nanorods.[42]

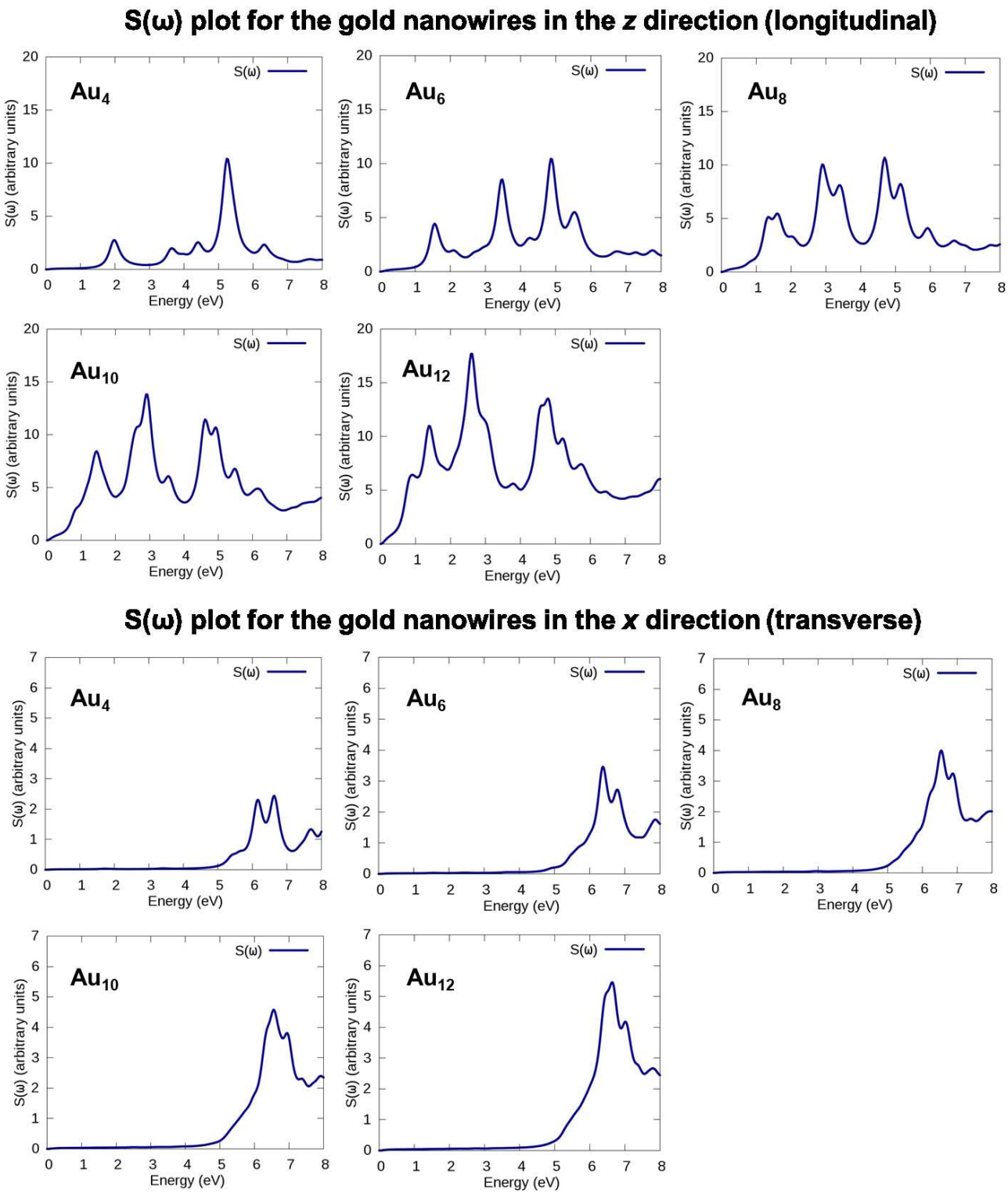

Figure 1. Optical absorption spectra for the longitudinal and transverse modes in the Au_m (m = 4, 6, 8, 10, 12) nanowires.

Longitudinal mode excitations

In gold, the 5d orbital energies are much closer to the energy of the 6s orbital compared to the 4d-5s energy difference in silver. Therefore, these energy differences are more likely to affect the optical properties in the visible range. Thus, developing an understanding of interband (d → sp) transitions originating from the d band of the gold nanowires is crucial because of the coupling of these transitions with intraband (sp → sp) transitions and their combined effects on the longitudinal and transverse mode frequencies and intensities.

As in the previous real-time study on related silver nanowires by Li and coworkers,[60] the time dependent occupation numbers of the orbitals responsible for the main peaks in the optical absorption spectrum are obtained by analyzing the evolution of the electron density via projection onto the ground state molecular orbital space. This approach is useful to understand the nature of the interplay between the single particle transitions involved in plasmon modes. This analysis is carried out for the longitudinal excitations to recognize the orbitals involved in the important transitions contributing to the longitudinal peaks. The respective orbital occupation number variations and their Fourier transformed spectra are shown in Fig. 2 for Au_4 and Au_6; we present pairs of orbitals that can be identified as strongly correlated transitions for the given longitudinal mode. Less strongly correlated transitions are shown in the SI (Fig. S2). The constructive and destructive nature of the electronic transitions can be obtained by the phase relationship between the time evolution of the orbital occupation numbers. If the orbital occupation number variations are in phase with the same frequency, they can constructively or destructively interact to give rise to several peaks in the optical absorption spectrum. In the longitudinal peaks of the current gold nanowire study, we observe a coupling of sp delocalized orbital transitions ($\Sigma_n \rightarrow \Sigma_{n+1}$; n is the axial quantum number) with the interband transitions (d → Σ_{n+1}) as explained in more detail below.

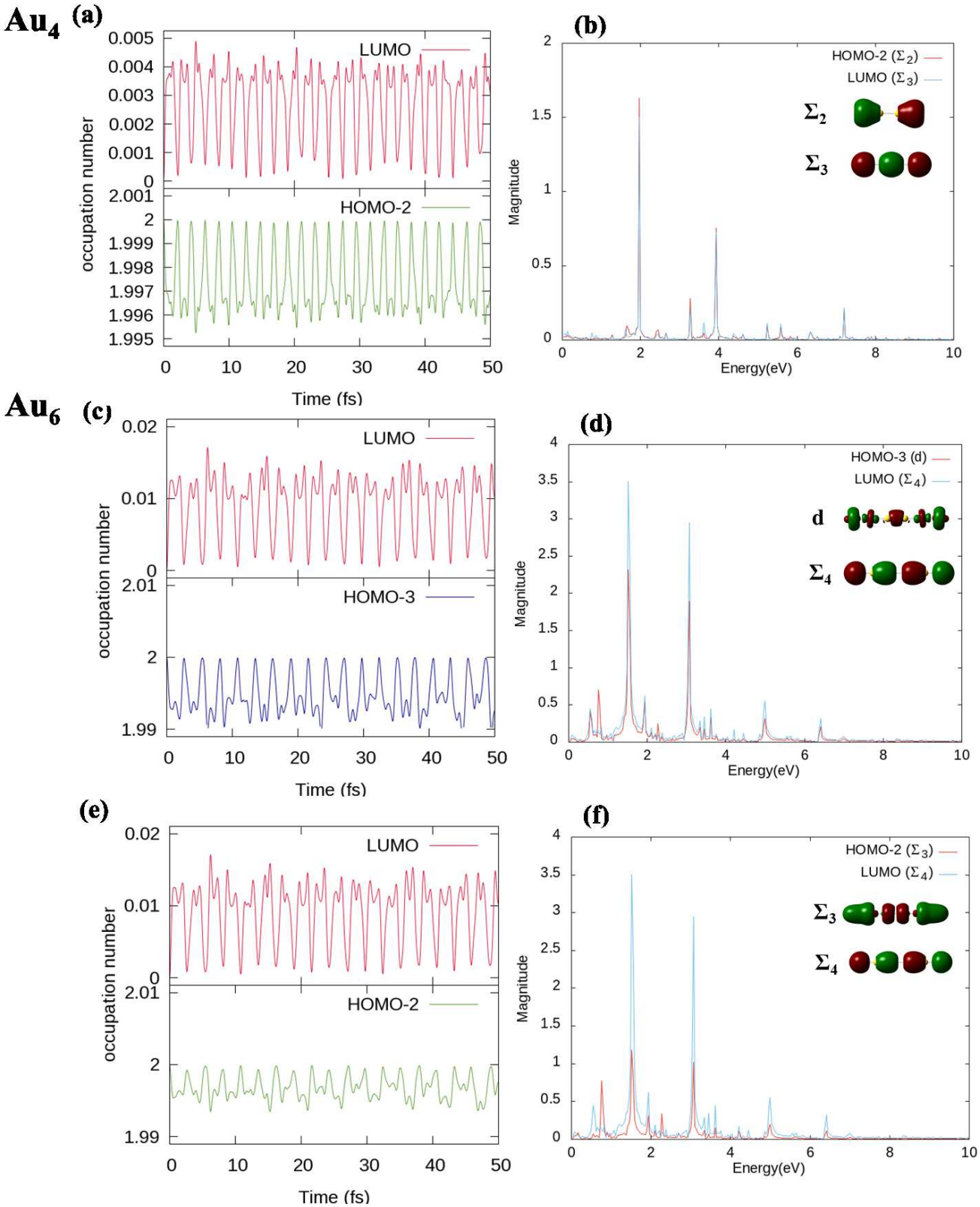
Au4
(a)
LUMO
HOMO-2
occupation number
Time (fs)
(b)
HOMO-2 (Σ2)
LUMO (Σ3)
Σ2
Σ3
Magnitude
Energy(eV)
Au6
(c)
LUMO
HOMO-3
occupation number
Time (fs)
(d)
HOMO-3 (d)
LUMO (Σ4)
d
Σ4
Magnitude
Energy(eV)
(e)
LUMO
HOMO-2
occupation number
Time (fs)
(f)
HOMO-2 (Σ3)
LUMO (Σ4)
Σ3
Σ4
Magnitude
Energy(eV)

Figure 2. Variations in orbital occupation numbers with time and their Fourier transformed spectra for strongly coupled orbital pairs in the longitudinal peaks of Au_m (m = 4, 6) nanowires. For Au_4, (a) shows the orbital occupation number variations for the two orbitals most responsible for the longitudinal peak and (b) shows their Fourier transformed spectra. Likewise, the c, d, e and f plots represent the orbital occupation number variations and their Fourier transformed spectra for Au_6. The strongest occupied-to-unoccupied transition is d → Σ_4 in plots c and d, and the e and f plots are for a less probable transition (Σ_3 → Σ_4).

Table 1. Single particle transitions involved in the longitudinal mode of gold nanowires determined by RT-TDDFT calculations.

Nanowire	Single particle transition	Symmetries
Au_4	HOMO-2 → LUMO	Σ_2 → Σ_3
Au_6	HOMO-2 → LUMO HOMO-3 → LUMO	Σ_3 → Σ_4 d → Σ_4
Au_8	HOMO-2 → LUMO HOMO-3 → LUMO	d → Σ_5 Σ_4 → Σ_5
Au_{10}	HOMO-3 → LUMO HOMO-4 → LUMO	d → Σ_6 Σ_5 → Σ_6
Au_{12}	HOMO-3 → LUMO HOMO-4 → LUMO HOMO-5 → LUMO	d → Σ_7 Σ_6 → Σ_7 d → Σ_7

In analyzing the real-time simulations of the longitudinal mode, this excitation is mainly constructed by one dominant single particle transition with a small contribution from one or two other single particle transitions as shown in Table 1. In agreement with previous work on gold nanowires, the Σ_n → Σ_{n+1} transition is an important component of the longitudinal excitations. In our current study, we also perform LR-TDDFT calculations with the same level of theory as our RT-TDDFT calculations in order to compare the excitations from the two methods directly. Both LR and RT calculations use the relativistic effects incorporated into the LanL2DZ basis set in the Gaussian software. The absorption spectra obtained by the LR-TDDFT method up to 7 eV are

shown in the supporting information (Fig. S1). The peak positions and the relative intensities of the absorption spectra obtained by LR and RT match well with each other.

The Kohn-Sham orbital energy diagram of the Au_4 nanowire obtained using the BP86/LanL2DZ level of theory is shown in Fig. 3. At this level of theory, the overlap of the d band with the sp-based Σ orbitals is clearly evident, which is reasonable for gold systems. This overlap with the d band increases the probability that hot carriers can be generated in both the sp band and the d band.

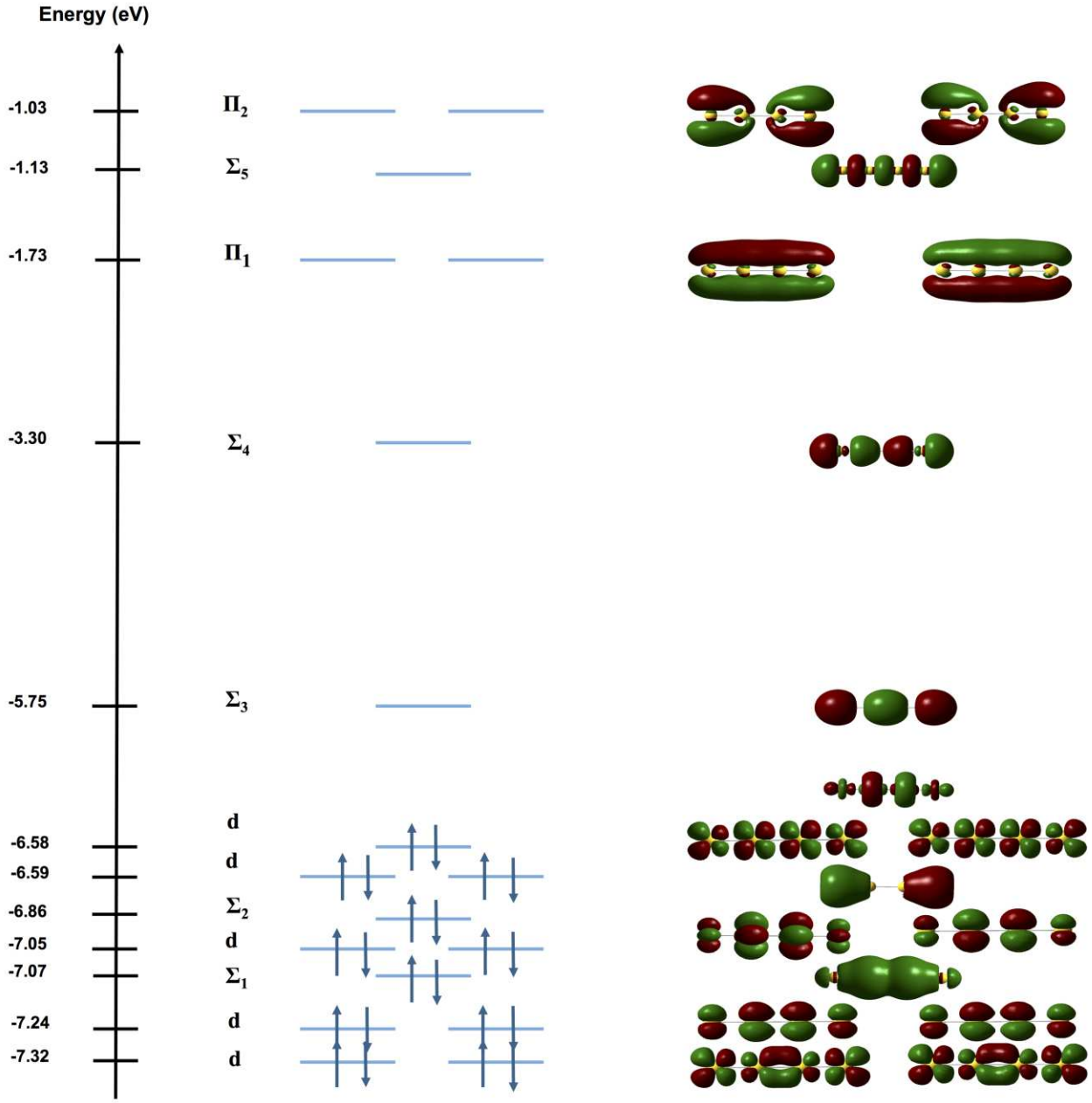

Figure 3. Kohn-Sham orbital energy diagram of Au_4.

In the Au_4 nanowire, the HOMO-2 → LUMO transition corresponds to a $\Sigma_2 \rightarrow \Sigma_3$ transition (Table 1). For the corresponding silver case, the strong excitation in Ag_4 also arises from a $\Sigma_2 \rightarrow \Sigma_3$ transition, although this corresponds to a HOMO → LUMO transition;[60] the difference in HOMO ordering is due to the presence of high-energy d band orbitals in the gold nanowire, as shown in Fig. 3. As shown in Fig. 2a, the orbital occupation numbers of the HOMO-2 and LUMO vary in phase and with the same frequency. They are strongly related and give rise to two intense peaks around 2 and 4 eV in the Fourier transformed spectrum. Therefore, it is evident that the HOMO-2 → LUMO transition ($\Sigma_2 \rightarrow \Sigma_3$) plays an important role in these two peaks in the Au_4 nanowire. However, the Fourier transformed off-diagonal element of the density matrix corresponding to this transition (Fig. S3) shows that only the peak at 2 eV results from this particular transition. This reveals that the peak appearing at 4 eV in the orbital occupation Fourier transforms is a result of a linear combination of the excitation energies (in this case, a 2ω peak where $\omega = 2$ eV) rather than an actual peak that would arise in the absorption spectrum. In that regard, the off-diagonal analysis provides more straightforward as well as more reliable information regarding the transitions responsible for the excitation peaks.

For comparison, the contributions of different single particle transitions can be determined from the eigenvectors in the LR-TDDFT calculations that provide the weights of each individual transition. Table 2 shows the LR-TDDFT excitation energies, oscillator strengths, single particle transitions, and the weights of each transition for both longitudinal and transverse modes for this nanowire. For the longitudinal modes, the HOMO-2 → LUMO transition possesses a high weight in the peak around 1.98 eV, which agrees with our assessment from the RT-TDDFT calculations. In the real-time simulation of the Au_4 nanowire we observe additional prominent peaks around 3.6, 4.4 and 5.2 eV in the longitudinal excitations of the optical absorption spectrum (Fig. 1a). The LR-TDDFT transitions in Table 2 indicate that there are excited states at 3.67, 4.43, and 5.29 eV. The 3.67 eV, 4.43 eV and 5.29 eV peaks are comparable with the real-time simulation peaks around the same energies. The RT-TDDFT peak positions differ slightly compared to the LR-TDDFT calculations due to the numerical precision available by reading off the peak positions from the dipole strength function in the RT approach, whereas the LR approach determines the excitation energies from eigenvalues of the Casida equation.

The peak at 5.2 eV has the highest intensity in the real-time simulation of the Au_4 longitudinal excitations (Fig. 1) which is also reflected in the LR-TDDFT calculation of a 5.29 eV excited state with a high oscillator strength (f=1.35) in Table 2. Those with the highest weights include HOMO-1 → LUMO+2 (two transitions due to degeneracies; each with a |weight| of 0.413), followed by HOMO-7 → LUMO+1 (0.217), HOMO → LUMO+3 (0.194), and HOMO-12 → LUMO (0.177). To understand the origin of this peak, the transitions involved in the 5.29 eV peak (Table 2) were further analyzed using the Fourier transformed spectra of the orbital occupation numbers from the RT-TDDFT calculations. The respective Fourier transformed spectra of the orbital occupation numbers are shown in the supporting information. As shown in Fig. S2, it is evident that the HOMO-12 → LUMO, HOMO-7 → LUMO+1, HOMO-2 → LUMO+3, HOMO-1 → LUMO+2, and HOMO → LUMO+3 transitions from the RT-TDDFT calculation are single particle transitions giving rise to the peak around 5.2 eV in the Fourier transformed spectra. This set of excitations includes many d→ sp interband transitions, including the dominant HOMO-1 → LUMO+2 transition. We have also analyzed the off-diagonal elements as shown in Fig. S4, and the analysis agrees with that from Fig. S2. The largest contribution to the peak arises from the HOMO-1 → LUMO+2 transition with smaller contributions from HOMO-12 → LUMO, HOMO-7 → LUMO+1, HOMO-2 → LUMO+3, and HOMO → LUMO+3. As noted above, the HOMO-1 → LUMO+2 transition, which is an interband transition, has a strong contribution to the 5.2 eV peak. It is evident that interband transitions are much more strongly involved in the electron dynamics of gold nanowires than in the corresponding silver nanowires.

Table 2. The LR-TDDFT excitation energies, oscillator strengths, single particle transitions and weights of each transition for longitudinal (L) and transverse (T) modes of Au_4 at the BP86/LanL2DZ level of theory. The "→/←" signs in the Transitions column indicate the excitations/de-excitations.

Peak	Energy (eV)	Oscillator strength	Transitions	Weight
L	1.98	0.39	HOMO-12 → LUMO	-0.161
			HOMO-2 → LUMO	0.712
			HOMO-2 ← LUMO	-0.201
	3.67	0.23	HOMO-12 → LUMO	0.623
			HOMO-7 → LUMO+1	0.270
			HOMO-4 → LUMO+1	-0.136

			HOMO-2 → LUMO	0.121
	4.43	0.27	HOMO-12 → LUMO	-0.214
			HOMO-7 → LUMO+1	0.570
			HOMO-4 → LUMO+1	-0.136
			HOMO-1 → LUMO+2	0.228
			HOMO-1 → LUMO+2 [a]	0.227
	5.29	1.35	HOMO-12 → LUMO	0.177
			HOMO-7 → LUMO+1	-0.217
			HOMO-2 → LUMO	0.138
			HOMO-2 → LUMO+3	0.136
			HOMO-1 → LUMO+2	0.413
			HOMO-1 → LUMO+2 [a]	0.413
			HOMO → LUMO+3	0.194
T	5.49	0.24	HOMO-1 → LUMO+2	-0.115
			HOMO-1 → LUMO+2 [a]	-0.115
			HOMO → LUMO+3	0.675
	6.2	0.25	HOMO-9 → LUMO+2	0.180
			HOMO-9 → LUMO+2	-0.179
			HOMO-8 → LUMO+5	-0.197
			HOMO-8 → LUMO+4	0.197
			HOMO-7 → LUMO+1	-0.124
			HOMO-6 → LUMO+3	-0.259
			HOMO-4 → LUMO+2	-0.217
			HOMO-3 → LUMO+4	-0.130
			HOMO-3 → LUMO+5	0.130
			HOMO-2 → LUMO+4	0.389
	6.38	0.22	HOMO-10 → LUMO+2	-0.134
			HOMO-10 → LUMO+2 [a]	-0.134
			HOMO-6 → LUMO+4	0.473
			HOMO-6 → LUMO+5	0.473
	6.7	0.3	HOMO-11 → LUMO+3	0.116
			HOMO-8 → LUMO+4	0.415
			HOMO-8 → LUMO+5	0.415
			HOMO-6 → LUMO+3	0.109
			HOMO-4 → LUMO+2	-0.114
			HOMO-2 → LUMO+5	0.243

[a]There are two components for this transition due to the degeneracy of the orbitals.

For Au_6, the HOMO-3 (d band orbital) is strongly correlated with the LUMO while the HOMO-2 (sp band orbital) is less strongly correlated with the LUMO (Fig. 2). The Fourier transformed spectrum of the orbital occupation numbers of HOMO-3 has peaks of similar magnitude to those of the LUMO, whereas the HOMO-2 has peaks with a smaller magnitude although they fall in the same frequency range of 1.5 – 4 eV. The orbital occupation number variation also shows that the HOMO-3 orbital occupation numbers vary in a larger range than for the HOMO-2. Therefore, the HOMO-3 → LUMO transition (d → Σ (sp) transition) appears to be the stronger transition involved in the longitudinal peaks of Au_6, while HOMO-2 → LUMO (which has $\Sigma_n \rightarrow \Sigma_{n+1}$ intraband character) contributes to a lesser extent; this is unique because all other gold nanowires examined in this study exhibit an intraband $\Sigma_n \rightarrow \Sigma_{n+1}$ transition as the strongest component of the excitation. LR-TDDFT calculations show that these two transitions can constructively add together to give rise to a strong peak near 1.5 eV, and this constructive interaction is identified by the hallmark of in-phase oscillations in the RT-TDDFT calculations that are apparent in Fig. 2. Furthermore, the Fourier transforms of off-diagonal elements corresponding to these two transitions in Fig. S5 clearly reflect that both these transitions cause the longitudinal peak, with the interband peak providing the largest contribution.

We have similarly performed RT-TDDFT calculations on longer chains to examine the electron dynamics in these systems. The Au_8, Au_{10}, and Au_{12} nanowires have HOMO-3 → LUMO, HOMO-4 → LUMO, and HOMO-4 → LUMO, respectively, as their most probable transitions in the longitudinal modes. Each of these transitions has $\Sigma_n \rightarrow \Sigma_{n+1}$ character. The d → Σ transitions are less probable transitions that contribute to the longitudinal excitations (Table 1). Real-time dynamics illustrating the transitions contributing to the longitudinal peaks of Au_8, Au_{10}, and Au_{12} are shown in Fig. S6, S8, and S10 respectively in supporting information. The corresponding off-diagonal analyses are given in Fig. S7, S9, and S11. In all cases, the electron dynamics in the gold nanowires are more complicated than those in the corresponding silver nanowires due to the involvement of interband transitions. Orbital occupation numbers are affected by all of these transitions and do not oscillate in a readily predictable manner. This suggests that RT-TDDFT calculations will provide an important tool for numerically simulating and understanding the complex real-time electron dynamics in these systems during processes such as plasmon decay and hot carrier generation.

Transverse mode excitations

Fig. 1f – j shows that the transverse modes of the gold nanowires display a band of several peaks in the energy range of 6-7 eV, which was also observed in previous LR-TDDFT calculations.[43] The transverse mode in the energy range of 6-7 eV displays two peaks; overall, the transverse peak intensity increases with the nanowire length. As the nanowire length increases from Au_4 to Au_{12}, the peak closer to 6 eV grows in intensity significantly while the peak closer to the 7 eV grows in intensity less noticeably.

In contrast to the longitudinal excitations that were dominated by a single intraband transition (albeit in combination with one or more interband transitions), the transverse modes in gold nanowires are constructed from a coupling of two or more single particle transitions with delocalized $\Sigma_n \rightarrow \Pi_n$ character (Fig. 4). The single particle transitions involved in the transverse mode of the gold nanowires are shown in Table 3. The involvement of two or more $\Sigma_n \rightarrow \Pi_n$ type single particle transitions in the transverse modes has also been observed in real-time simulations in related silver nanowires.[60] In the silver nanowire case, the strong transverse peak has been identified as arising from a superposition of $\Sigma_n \rightarrow \Pi_n$ single particle transitions. Their orbital occupation number variations are in phase with the same frequency and they constructively/destructively interact to give rise to several peaks in the transverse mode, which is supported by a configuration interaction (CI) picture arising from LR-TDDFT calculations.[60] In addition to the strong peaks around 5-7 eV, less intense peaks can be observed below 2 eV in the Fourier transforms of the occupation numbers (Fig. 4b and 4d). These peaks arise from energy differences between the plasmonic peaks.[60] They are more prevalent in these gold nanowires than in the corresponding silver chains because of the presence of a greater number of excited states in the gold systems due to the small 5d-6s gap.

Table 3. The single particle transitions involved in the transverse mode of gold nanowires obtained by RT-TDDFT calculations.

Nanowire	Single particle transition	Symmetries
Au_4	HOMO-2 → LUMO+4 HOMO-4 → LUMO+2	$\Sigma_2 \rightarrow \Pi_2$ $\Sigma_1 \rightarrow \Pi_1$
Au_6	HOMO-6 →LUMO+4	$\Sigma_2 \rightarrow \Pi_2$

	HOMO-9 → LUMO+3	$\Sigma_1 \rightarrow \Pi_1$
Au_8	HOMO-4 → LUMO+8 HOMO-9 → LUMO+5 HOMO-10 →LUMO+4	$\Sigma_3 \rightarrow \Pi_3$ $\Sigma_2 \rightarrow \Pi_2$ $\Sigma_1 \rightarrow \Pi_1$
Au_{10}	HOMO-9 → LUMO+9 HOMO-13 → LUMO+7 HOMO-16 → LUMO+6	$\Sigma_3 \rightarrow \Pi_3$ $\Sigma_2 \rightarrow \Pi_2$ $\Sigma_1 \rightarrow \Pi_1$
Au_{12}	HOMO-15 → LUMO+9 HOMO-17 → LUMO+7 HOMO-19 → LUMO+5	$\Sigma_3 \rightarrow \Pi_3$ $\Sigma_2 \rightarrow \Pi_2$ $\Sigma_1 \rightarrow \Pi_1$

Au_4

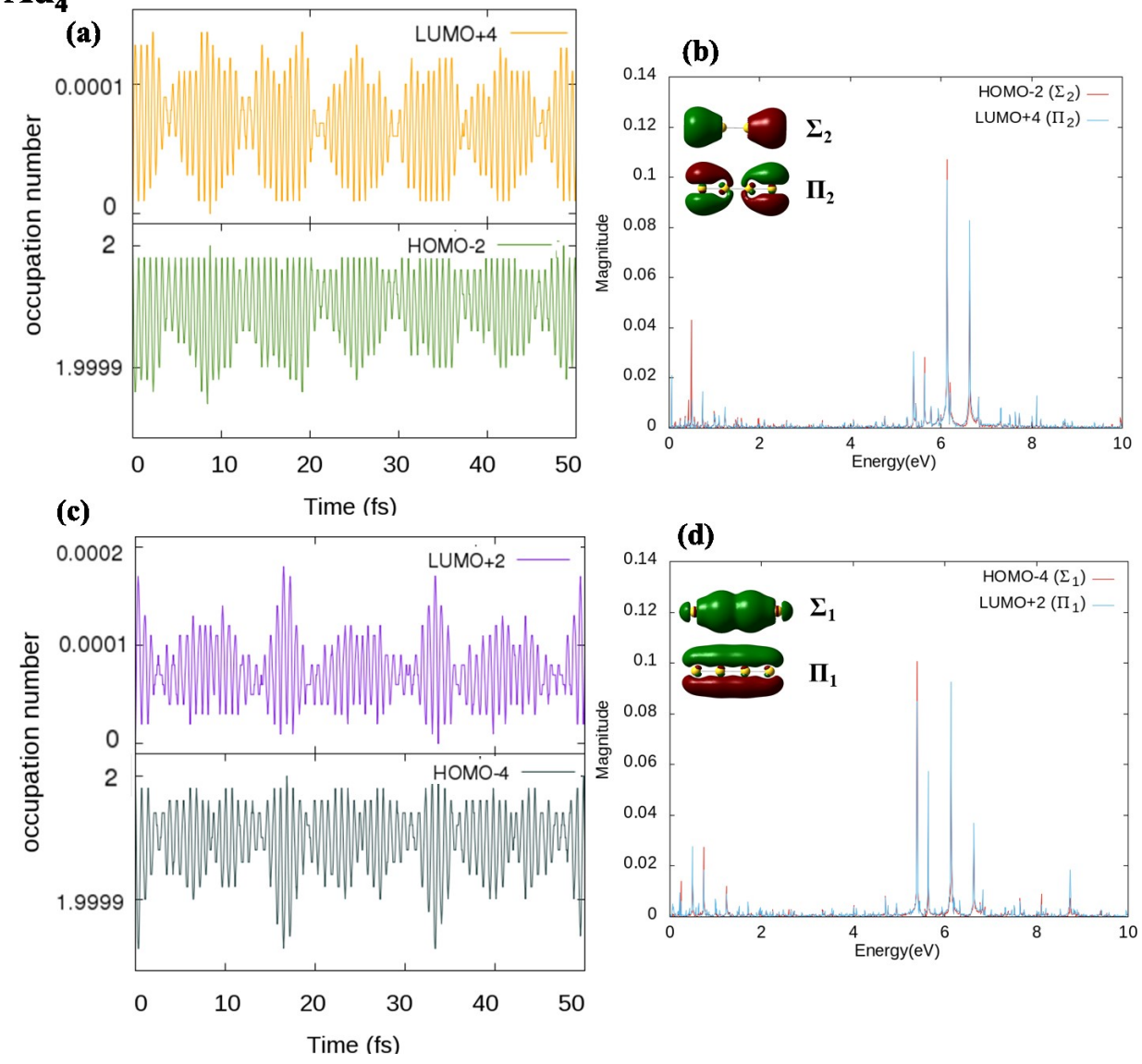

Figure 4. The orbital occupation number variation [a and c] and the respective Fourier transformed spectra [b and d] for strongly correlated transitions responsible for the transverse mode of Au_4.

Fig. 4 shows the orbital occupation number variation and the respective Fourier transformed spectra for the strongly correlated transitions for the transverse mode of Au_4. The data for Au_4 clearly indicates that the HOMO-2 → LUMO+4 ($\Sigma_2 \rightarrow \Pi_2$) and HOMO-4 → LUMO+2 ($\Sigma_1 \rightarrow \Pi_1$) transitions are the most probable due to the strong relationships between the respective orbital occupation number variations as shown in Figures 4a and c. The HOMO-2 and LUMO+4 orbital occupation numbers vary in phase and with the same frequency; the same is true for HOMO-4 and LUMO+2. The Fourier transformed spectra of the respective orbital occupation numbers (Fig. 4b, 4d) demonstrate peaks with a high magnitude around the 6–7 eV energy range, which supports the idea that those transitions are responsible for the transverse peaks that appear in the 6–7 eV range in the optical absorption spectrum of Au_4. We have also analyzed the Fourier transforms of the off-diagonal elements of the density matrix (Fig. S12) and these corroborate the findings from the orbital occupation number dynamics.

Table 2 also shows the energies, oscillator strengths, transitions and weights of the transitions involved in the Au_4 transverse mode from the LR-TDDFT calculations. It indicates three main peaks around 5.49, 6.20, 6.38 and 6.70 eV which are comparable to the main peaks around 5.4, 6.1 and 6.6 eV in the Au_4 optical absorption spectrum (Fig. 1f). The two intraband transitions HOMO-4 → LUMO+2 and HOMO-2 → LUMO+4 that are shown to be the primary contributors to the transverse peak from real-time simulations are also visible in the LR-TDDFT calculation as transitions that contribute to the transverse mode. However, their weights are not as high as those of the other transitions. (We have previously observed in other plasmonic systems that the weights of the transitions do not necessarily correlate with the transitions that contribute the most to the oscillator strength; the most important factor is the transition dipole moment calculated between the orbitals involved. For example, it is possible for an interband transition to have a large weight but a low contribution to the overall oscillator strength of the peak.) For Au_4, the other transitions involved in the LR-TDDFT transverse mode are also visible in the real-time calculations, which is evident from the Fourier transformed spectra of their orbital occupation numbers. However, the Fourier transformed spectrum of the orbital occupations for these interband

exhibit low magnitude peaks around the 6 – 7 eV energy range compared to the peaks related to the primary intraband transitions mentioned above. This supports the idea that the transverse mode of the gold nanowires is mainly constructed with $\Sigma_n \rightarrow \Pi_n$ type intraband transitions while other transitions such as interband transitions contribute to a lesser extent. Their orbital occupation numbers vary in phase with same frequency which is evident from the real-time calculations.

Similar behavior can be observed in the rest of the nanowires, as shown in Table 3. Their orbital occupation number variations and the Fourier transformed spectra for the strongly correlated transitions are shown in Fig. S13, S15, S17 and S19 in the supporting information. The corresponding off-diagonal analyses are given in Fig. S14, S16, S18 and S20. Again, the electron dynamics are more complicated than those of the corresponding silver nanowires due to the involvement of the interband transitions, although the transverse mode is still dominated by a constructive combination of intraband transitions that is primarily responsible for the transverse plasmon in these systems.

Conclusions

A series of linear gold nanowires having 4, 6, 8, 10 and 12 atoms were investigated using a RT-TDDFT method with a step function electric field perturbation. The aim of this work is to understand the differences in the plasmon-like character in gold nanowires compared to silver nanowires using the RT-TDDFT method and to investigate how the d band transitions play a role in determining the character of plasmon-like states in gold nanowires. Therefore, we studied the time evolution of the single particle transitions and examined the interplay between different transitions involved in the plasmonic excitations of model gold nanowires Au_m (m= 4, 6, 8, 10, 12).

The dipole strength functions (optical absorption spectra) were obtained for both longitudinal and transverse modes of the nanowires. The lowest-energy longitudinal peak appears in the energy range of 1-2 eV and redshifts with increasing nanowire length similar to previous LR-TDDFT calculations on gold nanowires as well as to RT and LR calculations on silver nanowires. A splitting is evident in the longitudinal peak with increasing nanowire length, which arises from the transitions originating from the d band. A transverse mode is present around the 6-

7 eV energy range of the optical absorption spectrum, which is constant as the length of the nanowire increases. In both longitudinal and transverse modes, the dipole strength increases as the nanowire length increases from Au_4 to Au_{12}.

The time dependent occupation numbers and the off-diagonal elements of the time-dependent density matrix are Fourier transformed, and their spectra are used to understand the nature of the interplay between the single particle transitions involved in both of the plasmon modes. This analysis recognized the orbitals responsible for the important transitions contributing to both the longitudinal and transverse modes. The single particle transitions can constructively/destructively interact with each other, as observed through orbital occupation number variations that are in phase with the same frequency. This gives rise to several peaks in the optical absorption spectrum.

A dominant single particle transition ($\Sigma_n \rightarrow \Sigma_{n+1}$) can be identified in the longitudinal mode of gold nanowires similar to the previous silver nanowire study. We also observe a coupling of the dominant single particle transition with the less probable d-band transitions that have $d \rightarrow \Sigma$ character. This behavior was true for all the gold nanowires considered in this study except for the Au_6 nanowire which gives $d \rightarrow \Sigma$ as the most dominant single particle transition. The involvement of these interband transitions complicates the electron dynamics compared to corresponding silver nanowires, and suggests that RT-TDDFT calculations that examine electron occupancy of orbitals in real-time are a useful tool for determining electron and hole dynamics. The transverse modes in gold nanowires are constructed from a coupling of two or more single particle transitions with $\Sigma_n \rightarrow \Pi_n$ character, which was also seen in the previous silver nanowire study. Interband transitions also contribute to the transverse mode, although this mode is dominated by the intraband transitions. The Fourier transforms of off-diagonal elements of the density corresponding to the transitions responsible for both longitudinal and transverse excitations reaffirm the validity of the findings based on the orbital occupation number variation with time.

Overall, the RT-TDDFT calculations on gold nanowires in this study have produced plasmon-like characteristics in agreement with the LR-TDDFT calculations performed on gold nanowires in the current and in previous work. This study further confirms that the RT-TDDFT method can reproduce results similar to the LR method for small gold systems (e.g. nanowires) in the weak perturbation regime which has been shown for silver systems previously. Therefore, the

findings from this study provide a foundation for future investigations of strong field perturbations on gold/silver systems to understand their plasmonic behavior under these conditions. Moreover, RT-TDDFT calculations can be employed to examine plasmon decay and hot carrier generation processes in real-time, and to understand the effects of intraband and interband transitions on these processes.

Supporting Information

The Fourier transformed spectra of the orbital occupation number variations for the peak around ~5.2 eV in the longitudinal excitations of Au_4, variations in orbital occupation numbers and off-diagonal elements of the density matrix with time and their Fourier transformed spectra for less strongly coupled orbital pairs in the longitudinal peaks of Au_m (m = 8, 10, 12) nanowires, and the orbital occupation number variations and their Fourier transformed spectra for the less strongly coupled transitions in the transverse mode of Au_m (m = 6, 8, 10, 12) nanowires. Coordinates for the nanowires examined in this work.

Acknowledgement

This material is based on work supported by the Department of Energy under grant DE-SC0012273. The computing for this project was performed on the Beocat Research Cluster at Kansas State University, which is funded in part by NSF grants CHE-1726332, CNS-1006860, EPS-1006860, and EPS-0919443. The development of the first-principles electronic dynamics is supported by the US Department of Energy (DE-SC0006863 to XL). The development of linear response TDDFT method for computational spectroscopy was supported by the National Science Foundation (CHE-1565520 to XL).

References

1. Haes, A. J.; Haynes, C. L.; McFarland, A. D.; Schatz, G. C.; Van Duyne, R. P.; Zou, S., Plasmonic Materials for Surface-enhanced Sensing and Spectroscopy. *MRS Bull.* **2005,** *30*, 368-375.
2. Kneipp, K.; Wang, Y.; Kneipp, H.; Perelman, L. T.; Itzkan, I.; Dasari, R. R.; Feld, M. S., Single Molecule Detection using Surface-Enhanced Raman scattering (SERS). *Phys. Rev. Lett.* **1997,** *78*, 1667-1670.
3. Nie, S.; Emory, S. R., Probing Single Molecules and Single Nanoparticles by Surface-enhanced Raman Scattering. *Science* **1997,** *275*, 1102-1106.
4. Michaels, A. M.; Nirmal, M.; Brus, L., Surface Enhanced Raman Spectroscopy of Individual Rhodamine 6G Molecules on Large Ag Nanocrystals. *J. Am. Chem. Soc.* **1999,** *121*, 9932-9939.

5. Hutter, E.; Fendler, J. H., Exploitation of Localized Surface Plasmon Resonance. *Adv. Mater.* **2004,** *16*, 1685-1706.
6. Mullin, J.; Valley, N.; Blaber, M. G.; Schatz, G. C., Combined Quantum Mechanics (TDDFT) and Classical Electrodynamics (Mie theory) Methods for Calculating Surface Enhanced Raman and Hyper-Raman Spectra. *J. Phys. Chem. A* **2012,** *116*, 9574-9581.
7. Saha, K.; Agasti, S. S.; Kim, C.; Li, X.; Rotello, V. M., Gold Nanoparticles in Chemical and Biological Sensing. *Chem. Rev.* **2012,** *112*, 2739-2779.
8. Tagar, Z. A.; Memon, N.; Agheem, M. H.; Junejo, Y.; Hassan, S. S.; Kalwar, N. H.; Khattak, M. I., Selective, Simple and Economical Lead Sensor based on Ibuprofen Derived Silver Nanoparticles. *Sens. Actuator B-Chem.* **2011,** *157*, 430-437.
9. Jiang, S.; Win, K. Y.; Liu, S.; Teng, C. P.; Zheng, Y.; Han, M.-Y., Surface-functionalized Nanoparticles for Biosensing and Imaging-guided Therapeutics. *Nanoscale* **2013,** *5*, 3127-3148.
10. Sun, Y., Conversion of Ag Nanowires to AgCl Nanowires Decorated with Au Nanoparticles and Their Photocatalytic Activity. *J. Phys. Chem. C* **2010,** *114*, 2127-2133.
11. Huang, X.; Neretina, S.; El-Sayed, M. A., Gold Nanorods: From Synthesis and Properties to Biological and Biomedical Applications. *Adv. Mater.* **2009,** *21*, 4880-4910.
12. Huang, X.; El-Sayed, I. H.; Qian, W.; El-Sayed, M. A., Cancer Cell Imaging and Photothermal Therapy in the Near-infrared Region by Using Gold Nanorods. *J. Am. Chem. Soc.* **2006,** *128*, 2115-2120.
13. Zhang, J. Z., Biomedical Applications of Shape-controlled Plasmonic Nanostructures: A Case Study of Hollow Gold Nanospheres for Photothermal Ablation Therapy of Cancer. *J. Phys. Chem. Lett.* **2010,** *1*, 686-695.
14. Parab, H. J.; Chen, H. M.; Lai, T.-C.; Huang, J. H.; Chen, P. H.; Liu, R.-S.; Hsiao, M.; Chen, C.-H.; Tsai, D.-P.; Hwu, Y.-K., Biosensing, Cytotoxicity, and Cellular Uptake Studies of Surface-modified Gold Nanorods. *J. Phys. Chem. C* **2009,** *113*, 7574-7578.
15. Hirakawa, T.; Kamat, P. V., Photoinduced Electron Storage and Surface Plasmon Modulation in Ag@ TiO_2 Clusters. *Langmuir* **2004,** *20*, 5645-5647.
16. Chen, Y.-S.; Choi, H.; Kamat, P. V., Metal-cluster-sensitized Solar Cells. A New Class of Thiolated Gold Sensitizers Delivering Efficiency Greater than 2%. *J. Am. Chem. Soc.* **2013,** *135*, 8822-8825.
17. El-Sayed, I. H.; Huang, X.; El-Sayed, M. A., Surface Plasmon Resonance Scattering and Absorption of Anti-EGFR Antibody Conjugated Gold Nanoparticles in Cancer Diagnostics: Applications in Oral Cancer. *Nano Lett.* **2005,** *5*, 829-834.
18. Jin, R.; Cao, Y.; Mirkin, C. A.; Kelly, K.; Schatz, G. C.; Zheng, J., Photoinduced Conversion of Silver Nanospheres to Nanoprisms. *Science* **2001,** *294*, 1901-1903.
19. Fedrigo, S.; Harbich, W.; Buttet, J., Collective Dipole Oscillations in Small Silver Clusters Embedded in Rare-gas Matrices. *Phys. Rev. B* **1993,** *47*, 10706.
20. Schmucker, A. L.; Harris, N.; Banholzer, M. J.; Blaber, M. G.; Osberg, K. D.; Schatz, G. C.; Mirkin, C. A., Correlating Nanorod Structure with Experimentally Measured and Theoretically Predicted Surface Plasmon Resonance. *ACS Nano* **2010,** *4*, 5453-5463.
21. Köller, L.; Schumacher, M.; Köhn, J.; Teuber, S.; Tiggesbäumker, J.; Meiwes-Broer, K., Plasmon-enhanced Multi-ionization of Small Metal Clusters in Strong Femtosecond Laser Fields. *Phys. Rev. Lett.* **1999,** *82*, 3783-3786.
22. Jain, P. K.; El-Sayed, M. A., Plasmonic Coupling in Noble Metal Nanostructures. *Chem. Phys. Lett.* **2010,** *487*, 153-164.
23. Mahmoud, M. A.; El-Sayed, M. A., Different Plasmon Sensing Behavior of Silver and Gold Nanorods. *J. Phys. Chem. Lett.* **2013,** *4*, 1541-1545.
24. Okamoto, H.; Imura, K., Visualizing the Optical Field Structures in Metal Nanostructures. *J. Phys. Chem. Lett.* **2013,** *4*, 2230-2241.

25. Chen, H.; Shao, L.; Li, Q.; Wang, J., Gold Nanorods and their Plasmonic Properties. *Chem. Soc. Rev.* **2013,** *42*, 2679-2724.
26. Polavarapu, L.; Liz-Marzán, L. M., Towards Low-cost Flexible Substrates for Nanoplasmonic Sensing. *Phys. Chem. Chem. Phys.* **2013,** *15*, 5288-5300.
27. Kelly, K. L.; Coronado, E.; Zhao, L. L.; Schatz, G. C., The Optical Properties of Metal Nanoparticles: The Influence of Size, Shape, and Dielectric Environment. *J. Phys. Chem. B* **2003,** *107*, 668-677.
28. Aikens, C. M., Electronic Structure of Ligand-passivated Gold and Silver Nanoclusters. *J. Phys. Chem. Lett.* **2010,** *2*, 99-104.
29. Morton, S. M.; Silverstein, D. W.; Jensen, L., Theoretical Studies of Plasmonics using Electronic Structure Methods. *Chem. Rev.* **2011,** *111*, 3962-3994.
30. Nordlander, P.; Prodan, E., Plasmon Hybridization in Nanoparticles Near Metallic Surfaces. *Nano Lett.* **2004,** *4*, 2209-2213.
31. Nordlander, P.; Oubre, C.; Prodan, E.; Li, K.; Stockman, M., Plasmon Hybridization in Nanoparticle Dimers. *Nano Lett.* **2004,** *4*, 899-903.
32. Jain, P. K.; El-Sayed, M. A., Surface Plasmon Resonance Sensitivity of Metal Nanostructures: Physical Basis and Universal Scaling in Metal Nanoshells. *J. Phys. Chem. C* **2007,** *111*, 17451-17454.
33. Link, S.; El-Sayed, M. A., Size and Temperature Dependence of the Plasmon Absorption of Colloidal Gold Nanoparticles. *J. Phys. Chem. B* **1999,** *103*, 4212-4217.
34. Gonzalez, A.; Noguez, C.; Ortiz, G.; Rodriguez-Gattorno, G., Optical Absorbance of Colloidal Suspensions of Silver Polyhedral Nanoparticles. *J. Phys. Chem. B* **2005,** *109*, 17512-17517.
35. Wiley, B. J.; Im, S. H.; Li, Z.-Y.; McLellan, J.; Siekkinen, A.; Xia, Y., Maneuvering the Surface Plasmon Resonance of Silver Nanostructures through Shape-Controlled Synthesis. *J. Phys. Chem. B* **2006,** *110*, 15666-15675.
36. Link, S.; Mohamed, M.; El-Sayed, M., Simulation of the Optical Absorption Spectra of Gold Nanorods as a Function of their Aspect Ratio and the Effect of the Medium Dielectric Constant. *J. Phys. Chem. B* **1999,** *103*, 3073-3077.
37. Al-Sherbini, E.-S. A., UV–visible Light Reshaping of Gold Nanorods. *Mater. Chem. Phys.* **2010,** *121*, 349-353.
38. Ni, W.; Ambjornsson, T.; Apell, S. P.; Chen, H.; Wang, J., Observing Plasmonic−molecular Resonance Coupling on Single Gold Nanorods. *Nano Lett.* **2009,** *10*, 77-84.
39. Yu, Y.-Y.; Chang, S.-S.; Lee, C.-L.; Wang, C. C., Gold Nanorods: Electrochemical Synthesis and Optical Properties. *J. Phys. Chem. B* **1997,** *101*, 6661-6664.
40. Pietrobon, B.; McEachran, M.; Kitaev, V., Synthesis of Size-controlled Faceted Pentagonal Silver Nanorods with Tunable Plasmonic Properties and Self-assembly of these Nanorods. *ACS Nano* **2008,** *3*, 21-26.
41. Liao, M.-S.; Bonifassi, P.; Leszczynski, J.; Ray, P. C.; Huang, M.-J.; Watts, J. D., Structure, Bonding, and Linear Optical Properties of a Series of Silver and Gold Nanorod Clusters: DFT/TDDFT Studies. *J. Phys. Chem. A* **2010,** *114*, 12701-12708.
42. Johnson, H. E.; Aikens, C. M., Electronic Structure and TDDFT Optical Absorption Spectra of Silver Nanorods. *J. Phys. Chem. A* **2009,** *113*, 4445-4450.
43. Guidez, E. B.; Aikens, C. M., Theoretical Analysis of the Optical Excitation Spectra of Silver and Gold Nanowires. *Nanoscale* **2012,** *4*, 4190-4198.
44. Piccini, G.; Havenith, R. W. A.; Broer, R.; Stener, M., Gold Nanowires: A Time-Dependent Density Functional Assessment of Plasmonic Behavior. *J. Phys. Chem. C* **2013,** *117*, 17196-17204.
45. Khan, S. A.; Senapati, D.; Senapati, T.; Bonifassi, P.; Fan, Z.; Singh, A. K.; Neeley, A.; Hill, G.; Ray, P. C., Size Dependent Nonlinear Optical Properties of Silver Quantum Clusters. *Chem. Phys. Lett.* **2011,** *512*, 92-95.

46. Koponen, L.; Tunturivuori, L. O.; Puska, M. J.; Hancock, Y., Tunability of the Optical Absorption in Small Silver Cluster-polymer Hybrid Systems. *J. Chem. Phys.* **2010,** *132*, 214301/1-8.
47. Aikens, C. M.; Li, S.; Schatz, G. C., From Discrete Electronic States to Plasmons: TDDFT Optical Absorption Properties of Ag_n (*n*= 10, 20, 35, 56, 84, 120) Tetrahedral Clusters. *J. Phys. Chem. C* **2008,** *112*, 11272-11279.
48. Bernadotte, S.; Evers, F.; Jacob, C. R., Plasmons in Molecules. *J. Phys. Chem. C* **2013,** *117*, 1863-1878.
49. Lian, K.-Y.; Sałek, P.; Jin, M.; Ding, D., Density-functional Studies of Plasmons in Small Metal Clusters. *J. Chem. Phys.* **2009,** *130*, 174701/1-6.
50. Yan, J.; Yuan, Z.; Gao, S., End and Central Plasmon Resonances in Linear Atomic Chains. *Phys. Rev. Lett.* **2007,** *98*, 216602-216605.
51. Yan, J.; Gao, S., Plasmon Resonances in Linear Atomic Chains: Free-electron Behavior and Anisotropic Screening of d Electrons. *Phys. Rev. B* **2008,** *78*, 235413-235422.
52. Gao, B.; Ruud, K.; Luo, Y., Plasmon Resonances in Linear Noble-metal Chains. *J. Chem. Phys.* **2012,** *137*, 194307/1-11.
53. Sinha-Roy, R.; García-González, P.; Weissker, H.-C.; Rabilloud, F.; Fernández-Domínguez, A. I., Classical and ab Initio Plasmonics Meet at Sub-nanometric Noble Metal Rods. *ACS Photonics* **2017,** *4*, 1484-1493.
54. Durante, N.; Fortunelli, A.; Broyer, M.; Stener, M., Optical Properties of Au Nanoclusters from TD-DFT Calculations. *J. Phys. Chem. C* **2011,** *115*, 6277-6282.
55. Harb, M.; Rabilloud, F.; Simon, D.; Rydlo, A.; Lecoultre, S.; Conus, F.; Rodrigues, V.; Félix, C., Optical Absorption of Small Silver Clusters: Ag_n,(*n*= 4–22). *J. Chem. Phys.* **2008,** *129*, 194108/1-9.
56. Kümmel, S.; Andrae, K.; Reinhard, P.-G., Collectivity in the Optical Response. of Small Metal Clusters. *Appl. Phys. B* **2001,** *73*, 293-297.
57. Bae, G.-T.; Aikens, C. M., Time-Dependent Density Functional Theory Studies of Optical Properties of Ag Nanoparticles: Octahedra, Truncated Octahedra, and Icosahedra. *J. Phys. Chem. C* **2012,** *116*, 10356-10367.
58. Guidez, E. B.; Aikens, C. M., Diameter Dependence of the Excitation Spectra of Silver and Gold Nanorods. *J. Phys. Chem. C* **2013,** *117*, 12325-12336.
59. Weerawardene, K. L. D. M.; Aikens, C. M., Comparison and Convergence of Optical Absorption Spectra of Noble Metal Nanoparticles Computed using Linear-Response and Real-Time Time-Dependent Density Functional Theories. *Comput. Theor. Chem.* **2018,** *1146*, 27-36.
60. Ding, F.; Guidez, E. B.; Aikens, C. M.; Li, X., Quantum Coherent Plasmon in Silver Nanowires: A Real-time TDDFT Study. *J. Chem. Phys.* **2014,** *140*, 244705/1-7.
61. Li, X.; Smith, S. M.; Markevitch, A. N.; Romanov, D. A.; Levis, R. J.; Schlegel, H. B., A Time-Dependent Hartree–Fock Approach for Studying the Electronic Optical Response of Molecules in Intense Fields. *Phys. Chem. Chem. Phys.* **2005,** *7*, 233-239.
62. Rossi, T. P.; Kuisma, M.; Puska, M. J.; Nieminen, R. M.; Erhart, P., Kohn–Sham Decomposition in Real-Time Time-Dependent Density-Functional Theory: An Efficient Tool for Analyzing Plasmonic Excitations. *J. Chem. Theor. Comput.* **2017,** *13*, 4779-4790.
63. Ma, J.; Wang, Z.; Wang, L.-W., Interplay between Plasmon and Single-Particle Excitations in a Metal Nanocluster. *Nat. Commun.* **2015,** *6*, 10107/1-11.
64. Bruner, A.; LaMaster, D.; Lopata, K., Accelerated Broadband Spectra Using Transition Dipole Decomposition and Padé Approximants. *J. Chem. Theor. Comput.* **2016,** *12*, 3741-3750.
65. Kresin, V. V., Collective Resonances in Silver Clusters: Role of d Electrons and the Polarization-free Surface Layer. *Phys. Rev. B* **1995,** *51*, 1844-1849.
66. Yabana, K.; Nakatsukasa, T.; Iwata, J. I.; Bertsch, G., Real-time, Real-space Implementation of the Linear Response Time-dependent Density-Functional Theory. *Phys. Status Solidi B* **2006,** *243*, 1121-1138.

67. Frisch, M.; Trucks, G.; Schlegel, H. B.; Scuseria, G.; Robb, M.; Cheeseman, J.; Scalmani, G.; Barone, V.; Mennucci, B.; Petersson, G., Gaussian 09, revision D. 01. Gaussian, Inc., Wallingford CT: 2009.
68. Smith, S. M.; Li, X.; Markevitch, A. N.; Romanov, D. A.; Levis, R. J.; Schlegel, H. B., A Numerical Simulation of Nonadiabatic Electron Excitation in the Strong Field Regime: Linear Polyenes. *J. Phys. Chem. A* **2005,** *109*, 5176-5185.
69. Smith, S. M.; Li, X.; Markevitch, A. N.; Romanov, D. A.; Levis, R. J.; Schlegel, H. B., Numerical Simulation of Nonadiabatic Electron Excitation in the Strong Field Regime. 2. Linear Polyene Cations. *J. Phys. Chem. A* **2005,** *109*, 10527-10534.
70. Becke, A. D., Density-functional Exchange-energy Approximation with Correct Asymptotic Behavior. *Phys. Rev. A* **1988,** *38*, 3098-3100.
71. Perdew, J. P., Density-functional Approximation for the Correlation Energy of the Inhomogeneous Electron Gas. *Phys. Rev. B* **1986,** *33*, 8822-8824.
72. Hay, P. J.; Wadt, W. R., Ab initio Effective Core Potentials for Molecular Calculations. Potentials for K to Au Including the Outermost Core Orbitals. *J. Chem. Phys.* **1985,** *82*, 299-310.
73. Hay, P. J.; Wadt, W. R., Ab initio Effective Core Potentials for Molecular Calculations. Potentials for the Transition Metal Atoms Sc to Hg. *J. Chem. Phys.* **1985,** *82*, 270-283.
74. Wadt, W. R.; Hay, P. J., Ab initio Effective Core Potentials for Molecular Calculations. Potentials for Main Group Elements Na to Bi. *J. Chem. Phys.* **1985,** *82*, 284-298.
75. Martin, R. M., *Electronic Structure: Basic Theory and Practical Methods*. Cambridge University Press, Cambridge, UK: 2004.
76. Lenthe, E. v.; Baerends, E.-J.; Snijders, J. G., Relativistic Regular Two-component Hamiltonians. *J. Chem. Phys.* **1993,** *99*, 4597-4610.
77. Te Velde, G. t.; Bickelhaupt, F. M.; Baerends, E. J.; Fonseca Guerra, C.; van Gisbergen, S. J.; Snijders, J. G.; Ziegler, T., Chemistry with ADF. *J. Comput. Chem.* **2001,** *22*, 931-967.

TOC Graphic

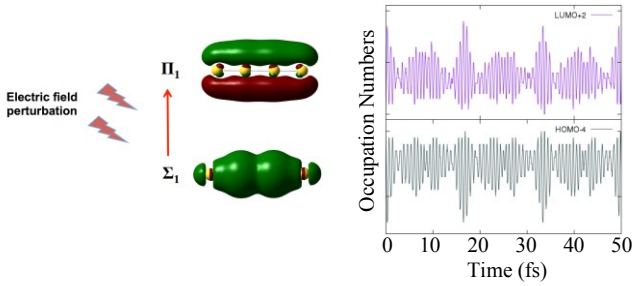
Electric field
perturbation
Π1
Σ1
LUMO+2
HOMO-4
Occupation Numbers
0
10
20
30
40
50
Time (fs)